Acoustic Emission Monitoring of a Reinforced Concrete Shear Wall by b-value based Outlier Analysis

Alireza Farhidzadeh, Salvatore Salamone, Bismarck Luna and Andrew Whittaker

Structural Health Monitoring published online 17 September 2012
DOI: 10.1177/1475921712461162

Article

Structural Health Monitoring

Structural Health Monitoring
0(0) 1–11

DOI: 10.1177/1475921712461162
shm.sagepub.com
SAGE

Acoustic emission monitoring of a reinforced concrete shear wall by *b*-value–based outlier analysis

Alireza Farhidzadeh[1], Salvatore Salamone[1], Bismarck Luna[2] and Andrew Whittaker[2]

Abstract

Reinforced concrete shear walls are critical structural components in gravity and lateral force resisting systems. The objective of this work is to design and validate a monitoring system capable of rapid and automated damage assessment of reinforced concrete shear walls. The proposed system is based on a sparse array of piezoelectric transducers to receive acoustic emissions distributed across the wall and a statistical pattern recognition algorithm capable of identifying critical structural conditions to inform decision makers on the need for repair to ensure safe operation of the structure. The proposed system was validated on a full-scale reinforced concrete shear wall subjected to quasi-static cyclic loading.

Keywords

Acoustic emission, reinforced concrete shear wall, *b*-value analysis, outlier analysis

Introduction

Reinforced concrete (RC) shear walls are popular gravity and lateral force resisting systems. Failure of a shear wall could result in severe damage and even progressive collapse of a concrete structure. Currently, the vast majority of postevent inspections are visual, and unfortunately, even with the recent advances in automated ground-based nondestructive evaluation (NDE) methods, there is a potential that indications of structural degradation could be missed. Structural safety inspections can be difficult and tedious because (a) the feature sizes for cracks and corrosion are often small with respect to the resolution of the inspection methods, (b) crucial structural details are often hidden or buried inside surrounding structure, making access difficult, and (c) inspection of structural components must include large areas with many features to inspect. For these reasons, structural health monitoring (SHM) capability has become more attractive for application in civil structures. In fact, prevention of unexpected structural failure could be improved by equipping structures with sensing and analysis systems to enable real-time, continuous, and autonomous monitoring. Furthermore, such systems, coupled with remote facilities, could be employed to overcome hundreds of inspection obstacles stemming from accessibility restrictions, complex geometries, and the location and depth of hidden damage. A technique that shows promise for monitoring concrete structures is the acoustic emission (AE) method. In general, AEs are stress waves caused by sudden strain releases due to internal fracture such as concrete cracking.[1] When a material is overstressed, a burst of energy is released in the form of high-frequency sound waves from propagating cracks or from plastic deformation.[2] Generally, a sparse array of piezoelectric transducers is placed in contact with the structure to detect these waves. By filtering out the background noise from AE, the damage states of a structure can be estimated. Several studies have demonstrated the ability of the AE to perform the

[1]Smart Structures Research Laboratory (SSRL), Department of Civil, Structural, and Environmental Engineering, University at Buffalo, the State University of New York, Buffalo, NY, USA
[2]Department of Civil, Structural, and Environmental Engineering, State University at Buffalo, the State University of New York, Buffalo, NY, USA

Corresponding author:
Salvatore Salamone, Smart Structures Research Laboratory (SSRL), Department of Civil, Structural, and Environmental Engineering, University at Buffalo, the State University of New York, 212 Ketter Hall, Buffalo, NY 14260, USA.
Email: ssalamon@buffalo.edu

critical tasks of detection, location, and determination of the dynamics of cracks that may substantially degrade a structure and its ability to perform as intended.[3,4] Ohno and Ohtsu[5] proposed two crack classification methods to evaluate properly crack propagation and resultant degradation in concrete structures. One of them is a parameter-based method (parameter analysis) that has been carried out by employing two parameters of the average frequency and the RA value (i.e. the ratio of signal's rise time to its peak amplitude). The other crack classification is the simplified Green's functions for moment tensor analysis (SiGMA), which is known as a signal-based method.[6] The close similarity between AE generated by materials undergoing brittle failure and seismic waves generated by earthquakes triggered the use of seismological techniques such as *b*-value analysis in AE.[7,8] Colombo et al. used *b*-value analysis as an alternative way to process and interpret data recorded by eight sensors during a laboratory test on an RC beam and proposed some quantitative damage criteria.[9] Kurz[10] used the *b*-value and the improved *b*-value (*Ib*)[11] on a concrete beam and a concrete cube to connect stress redistribution to *b*-value drop and macrocrack growth in fracture process. Experimental studies have also been performed to recognize defect size distributions in concrete structures by *b*-value analysis.[12] Schumacher et al.[13] proposed a minimum *b*-value analysis to estimate the load capacity of bridge girders. Although AE-based techniques have several advantages, there are still some key disadvantages to its use. The primary disadvantage is that the AE data normally contain significant high-frequency noise, primarily caused by surrounding operational conditions (i.e. temperature and environmental noise) and the measurement equipment (e.g. preamplifiers that usually amplify the surrounding noise). Statistical-based pattern recognition algorithms therefore need to be implemented to automatically extract signal features and to recognize, classify, and interpret the results. This article investigates the monitoring of the fracture process in a large-scale RC shear wall using *b*-value analysis. In addition, a statistical pattern recognition technique based on an outlier analysis is proposed for identifying the initiation of serious damage of the shear wall caused by a significant change in its mechanical properties. Such a system if deployed widely could inform decision makers about the need for repair or to ensure the safe and reliable operation of critical structural systems.

Experimental test setup

Test specimen and load protocol

The test specimen was a large-scale rectangular shear wall with a height to width ratio of 0.54, designed based on ACI318-08, (chapter 21, earthquake-resistance structures)[14]. The width and thickness of the specimen were 305 cm (120 in) and 20.3 cm (8 in), respectively. The compressive strength of concrete was approximately 35 MPa (5.1 kips) after 28th day and was 48.2 MPa (7 kips) in the test day. The horizontal and vertical reinforcement ratio was 1%. The yield and ultimate strength of the reinforcing bars were 434 and 460 MPa, respectively. There were mechanical splices on the vertical rebar at approximately 35.6 cm (14 in) from the foundation. The specimen was rigidly connected to the laboratory's foundation using 14 Dywidag bars with a 1.5-in nominal diameter. The lateral load was applied to the specimen by two horizontally inclined high-force capacity actuators. The actuators were attached to the specimen through custom-made brackets and plates that were posttensioned to the sides of the specimen. The centerline of loading was at 165 cm (65 in) from the base. The specimen was subjected to a displacement-controlled quasi-static reversed cyclic loading. The loading protocol consisted of 11 load steps (LSs). The first LS had three cycles and the subsequent LSs had two cycles (C1, C2). Each cycle consisted of two phases, namely, positive load peak (PLP) and negative load peak (NLP), as shown in Figure 1. The loading rate was set at around 0.13 cm/s. The wall was displaced in the plane of its web. After reaching the peak in every cycle, the actuators load was maintained for approximately 20 min to map cracks propagation and take photos. More details on this wall can be found in Ref. 15.

AE system

The main components of the AE system included an eight-channel high-speed data acquisition board (Physical Acoustics Corporation Micro-II PAC) and dedicated software for signal processing and storage

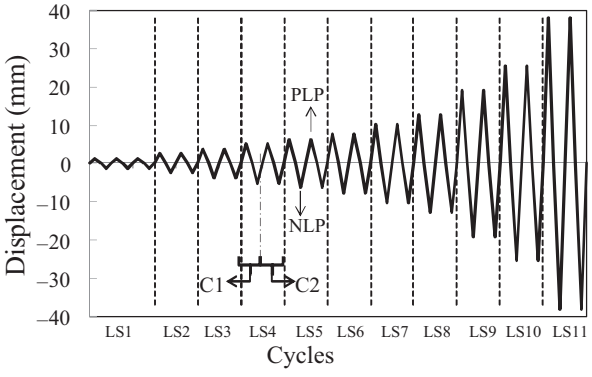

Figure 1. Load protocol.[15]
PLP: positive load peak; NLP: negative load peak; LS: load step.

(AEwin). The test specimen was instrumented with eight AE sensors (four R15α and four R6α) on one side of the wall. The sensors were attached to the face of the wall using hot glue. The AE sensors were used in conjunction with preamplifiers set at 40 dB gain and analog band-pass filters set in the interval of 20–400 kHz. In general, a trigger level can be set separately for each of the eight channels. When the amplitude of a trigger signal from any one of the eight AE transducers exceeds the preset level, the data signals from all transducers are digitized, saved, and transferred to a laptop computer. In this work, the trigger level was set to be 6 dB above the noise level of the system, which was determined as follows. The trigger level was gradually increased until the system began to capture signals continuously. This level was then taken as the noise level of the system, and the dominant source was assumed to be electronic noise in the preamplifier. During the test, the output from load cells was continuously recorded and correlated with the AE signals as a parametric input. The sensor layout as well as an overview of the experimental setup is schematically shown in Figure 2. Sensors were placed with spacing of 0.5 m based on attenuation measurements performed through pencil lead breaks at systematic grid locations. The estimated attenuation coefficient was about 29 dB/m.

AE-based outlier analysis

AE technique

The AE method exploits the propagation of transient elastic waves generated by the rapid release of energy from a localized source or sources within a specific material. The elastic energy propagates as a stress wave in the structure and is detected by one or more AE sensors. AE signals may be generated by crack onset, growth and propagation, rebar breaks, debond, and plastic deformations.[2,16] Characterizing the nature of AE sources is an open discussion in the scientific literature due to the complexity of the AE signals. They are affected by several factors, including (a) characteristics of the source, (b) the path taken from the source to the sensor, (c) the sensor's characteristics, and (d) the measuring system.[17,18] Generally, some relevant features such as maximum amplitude of the signal, energy of the signal, duration, and rise time are extracted from the AE signals to identify the sources and to evaluate their significance. Extracting parameters from the AE waveform is usually referred to as the parameter-based AE technique. In general, these features provide an indication of source intensity or severity. This is useful information for determining whether the test specimen is accumulating damage and, in turn, for deciding whether the test should continue or if the structure in question should remain in service. For example, several studies have shown that during the process of fracture of a concrete specimen, there is a relationship between types of cracks and AE frequency–amplitude distribution. Microcracks usually generate a large number of events of small amplitude, while macrocracks generate fewer events but of larger amplitude. When the cracks are opening up, as most of the energy has already been released, many events are created, but of a small amplitude. The *b*-value analysis can take all these considerations into account and it can then be used to monitor the fracture in concrete structures.

Introduction to b-value analysis

The *b*-value is obtained using the frequency–magnitude distribution data by means of Gutenberg–Richter

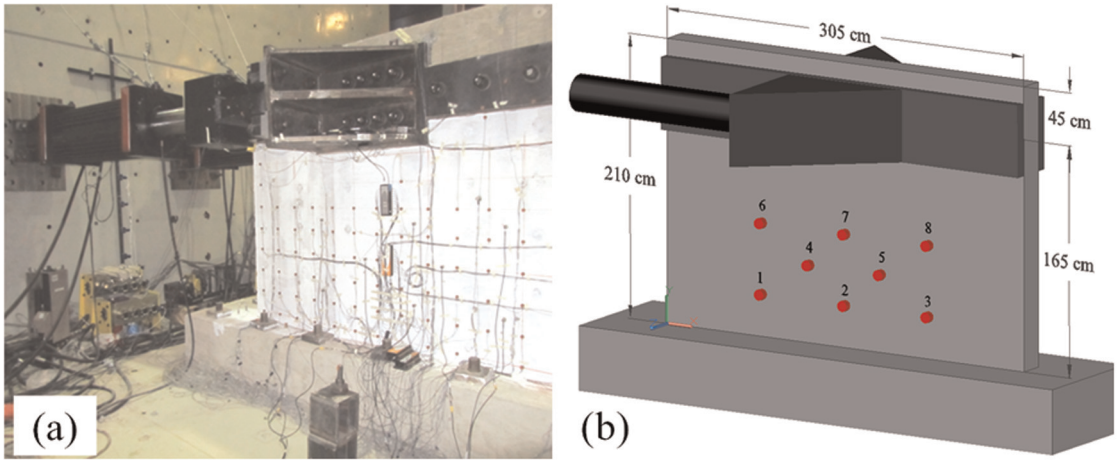

Figure 2. Experimental setup: (a) site view and instrumentation and (b) schematic AE transducer locations.
AE: acoustic emission.

relationship,[7] which is generally used in seismology to characterize distributions of earthquake magnitude. This relationship is defined as

$$\log_{10} N = a - bM \quad (1)$$

where M is the Richter magnitude of events, N is the incremental frequency (i.e. the number of events with magnitude in the range of $M \pm \Delta M/2$),[8] and a and b are both empirical constants to be estimated from the linear curve fitting; a is the intercept of the line with log N axis and b is the slope. The incremental frequency is also defined as the number of events with magnitude greater than M in literature;[7,10,11] the former definition is used in this article. Magnitude M is proportional to the logarithm of the maximum amplitude (A_{max}) recorded in a seismic trace and also to the logarithm of the source rupture area. Equation (1) has been also found to be valid for AE data, after dividing the AE peak amplitude by a factor of 20; this is because the AE peak amplitude is measured in decibel, whereas the Richter magnitude of earthquake is defined in terms of the logarithm of maximum amplitude. Therefore, equation (1) in terms of AE technique is modified as

$$\log_{10} N = a - b\left(\frac{A_{dB}}{20}\right) \quad (2)$$

where A_{dB} is the peak amplitude of AE event in decibel. Several studies have shown that during the fracture process in a concrete specimen, there is a relationship between the type of crack and the b-value. In general, the b-value increases during the nucleation of microcracks and decreases during the subsequent coalescence of these microcracks with macrocracks. The b-value analysis of AEs is usually applied to a certain number n of AE signals. Suggested values for n found in the literature range from 50 to 100.[19] However, recent studies have shown that this number n has to be verified because this parameter can influence the results.[20] To show the variability of the b-value with n, the total number of AE signals recorded during a loading cycle was divided into groups of different sizes ($n = 50$, $n = 70$, and $n = 100$) and the range of amplitude was decided to be in steps of 5 dB from the threshold to the maximum amplitude in the group. For each group, the log frequency–magnitude graph was plotted and their linear trend calculated using the least squares method of fitting curves.[9] The slope of such curves represents the b-value. The results are shown in Figure 3 as an example. It can be observed that using groups formed by a different number of events might affect the results. This variability introduces further uncertainties in the decision-making process. In addition, another issue in applying the technique is how to differentiate the AE signal of interest, that is, those due to crack growth or imminent failure, from noise of various natures in a large dataset. Often the real AE signals are measured in the presence of noise due to vibration, fretting, and electromagnetic interference, and therefore, automatic noise rejection is required before correlating AE activities with crack initiation or progressive failure. There is a need to develop algorithms capable of automatically classifying the level of damage despite variations in operating conditions of the structure. In constructing an SHM system that can interpret measured data and judge whether the condition of the structure has deviated substantially from its normal operational condition, a statistical approach based on an outlier analysis is proposed.

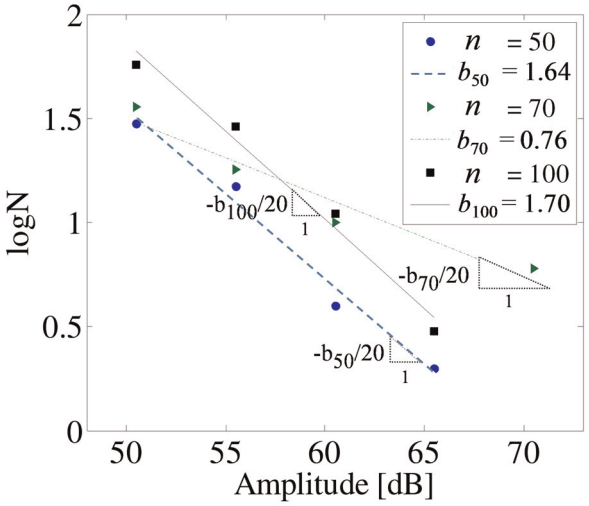

Figure 3. Log frequency–amplitude diagram, linear curve fitting and b-value calculation for different group sizes of n.

Outlier analysis background

The outlier analysis has been applied extensively in the field of ultrasonic testing,[20–25] but the use of this method to characterize AEs has not been fully investigated. An outlier is a datum that appears inconsistent with a set of baseline data. The baseline data describe the normal operating condition of the structure under investigation. Ideally, the baseline data should include the statistical variation of sensitive features due to normal changes in environmental and operational conditions of the structure (e.g. temperature, humidity, loading) and can be constructed based on the AE events recorded during the first year of operation of a new structure. For the sake of completeness, a brief introduction of the outlier analysis is provided below. For a more extensive review, the reader is referred to Barnett and Lewis.[26] In the analysis of univariate data, the detection of outliers is a straightforward process based upon the determination of the discordancy

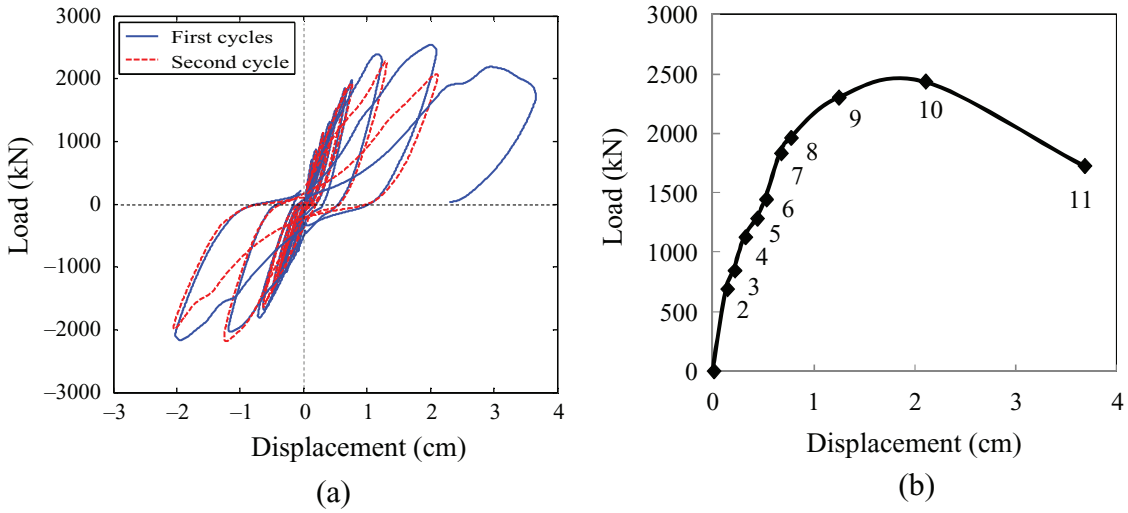

Figure 4. Structural response: (a) force–displacement hysteresis loop and (b) backbone curve.

between a single observed datum and the baseline statistics. One of the most common discordancy tests is based on deviation statistics, defined as

$$z_\zeta = \frac{|x_\zeta - \bar{x}|}{s} \quad (3)$$

where x_ζ is the potential outlier; $\bar{x}$ and s are the mean and the standard deviation of the baseline, respectively; and z_ζ quantifies the extent of discordance. The value of z_ζ is then compared to a defined threshold value, to determine whether the datum x_ζ is an outlier (i.e. above the threshold) or not. The mean and standard deviation can be calculated with or without the potential outlier, depending upon whether inclusive or exclusive measures are preferred. The inclusive manner of baseline computation was employed in this work. In this study, the baseline set incorporates b-values calculated from AE measurements acquired during the first cycle of the LS2 (LS2-C1). During the test, the b-values were extracted from each group of AE received. For a given observation, the discordancy value, calculated using equation (3), was compared with a threshold value in order to classify the observation as an anomaly (i.e. outlier) or normal operating conditions of the system (inlier). A Monte Carlo simulation was employed to compute the threshold. When baseline measurements are limited, a Monte Carlo simulation is an effective method for generating a large number of random data to populate the baseline distribution.[27]

Experimental results

Structural response

The structural response of the test specimen measured by force–displacement hysteresis loops and its corresponding backbone curve in the PLP are illustrated in Figure 4. In particular, since there are two cycles per LS, in Figure 4(a), the force–displacement hysteresis loops are shown for both first cycle (solid line) and second cycle (dashed line). It can be observed that in each LS, the second cycle shows less strength for a given lateral displacement. This can be due to the fact that majority of cracks are formed during the first cycle, and as a result, less force is required for achieving the same displacement in the subsequent cycle. Furthermore, from the backbone curve in Figure 4(b), it can be observed that significant nonlinear behavior of the wall started from LS8. In LS10, the wall reached to its maximum capacity, and in LS11, the wall lost significant strength. Table 1 summarizes the changes in mechanical properties of the wall during the test. In particular, the second column (strength) shows the force in the corresponding peak displacement and the third column calculates the relative strength to the maximum capacity recorded in LS10. The fourth column is the secant stiffness of the wall calculated by dividing the force by the corresponding peak displacement, and the fifth column is the percentage of stiffness with respect to LS2. In the onset of nonlinearity, LS8, 19% of the peak strength remained and the stiffness decreased to 50% of the stiffness measured at LS2, as can be seen in Table 1. Figure 5 shows representative pictures of cracks developed near one of the bottom corners during different stages of the loading process. These photos were taken when the wall was in PLP of the first cycle. It can be observed that during the early stages of the experiment (LS1, LS2, LS3, LS4), cracks were barely visible (i.e. microcracks). From LS5 onward, more visible cracks appeared and could be detected on the wall easily (i.e. macrocracks). At LS9, the width of most of cracks was more than 1 mm, and in LS10, the wall

Table 1. Mechanical properties of the shear wall during the load steps

Load step	Strength (kN)	Relative strength to LS10 (%)	Stiffness (kN/m)	Relative stiffness to LS2 (%)
LS2	691	28	51,898	100
LS3	846	35	41,007	79
LS4	1127	46	36,067	69
LS5	1283	53	29,914	58
LS6	1445	59	27,870	54
LS7	1834	75	27,578	53
LS8	1962	81	25,696	50
LS9	2302	94	18,610	36
LS10	2436	100	11,634	22
LS11	1726	71	4703	9

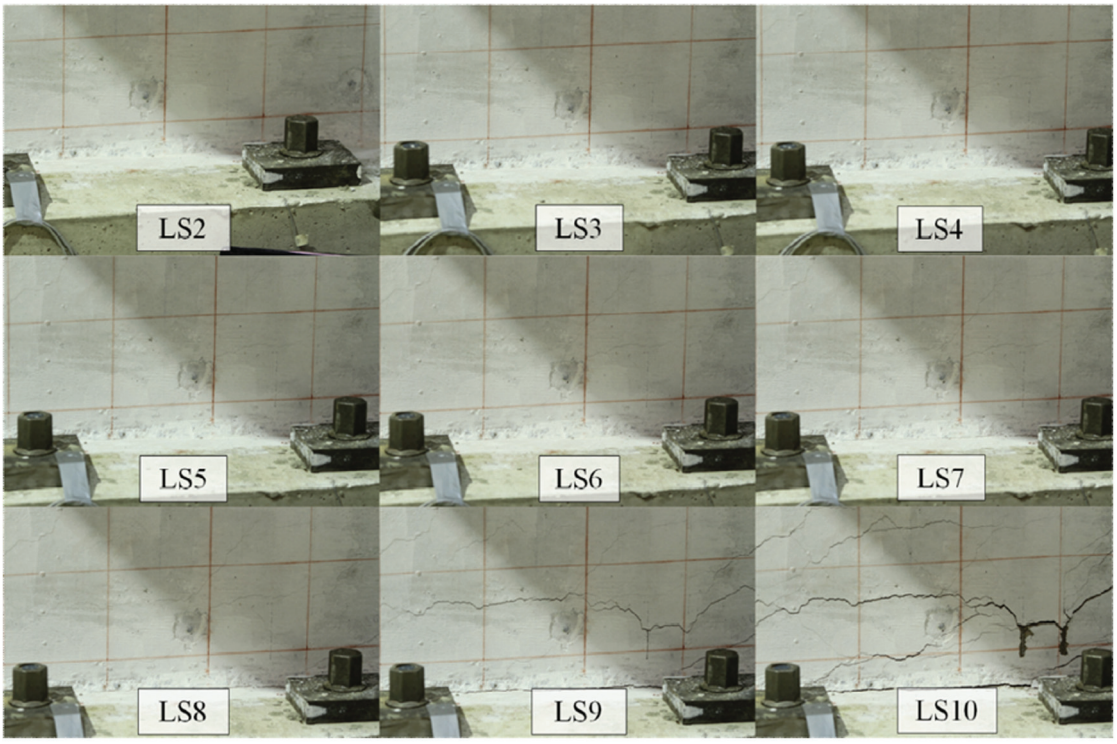

Figure 5. Crack status near bottom corner of the wall for the LSs of the first cycle.[28]
LS: load step.

appeared significantly damaged. It can be observed that a normal visual inspection may not be able to identify the onset of nonlinearity in LS8 because after the earthquake, the walls show only residual deformations and not peak deformation. Furthermore, even in peak deformation, the crack widths might be considered acceptable, as shown in Figure 5. The observed fracture process was compared with *b*-value analysis results in section "*b*-value results."

AE results

Representative results from the AE monitoring of the test specimen are illustrated in this section. Figure 6 shows the amplitudes of AE signals recorded from all sensors during the first and second cycles for each LS. In the data processing, the LS1 was ignored as the number of AE signals was not significant. The load history recorded by the actuators load cells (i.e. solid line)

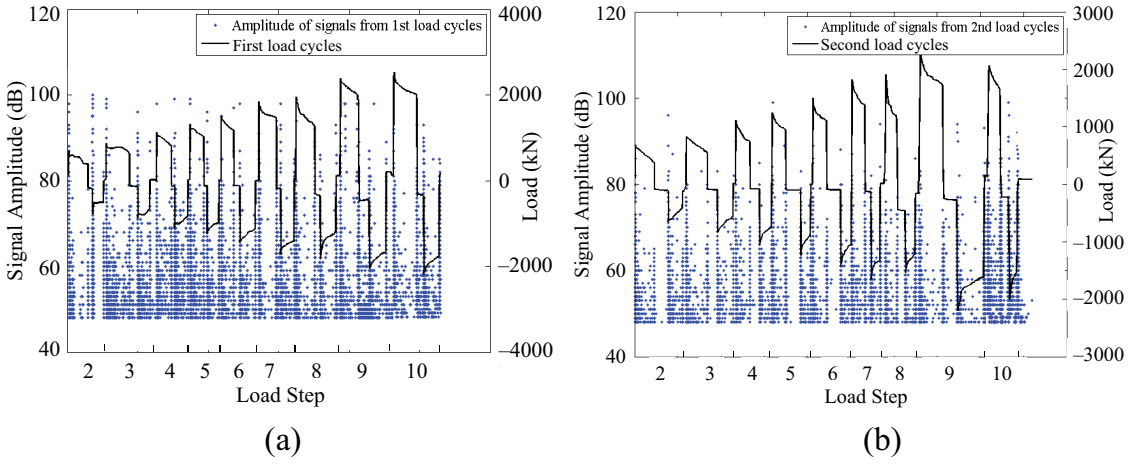

Figure 6. Peak amplitude of AE signals during the test: (a) first cycle and (b) second cycle.
AE: acoustic emission.

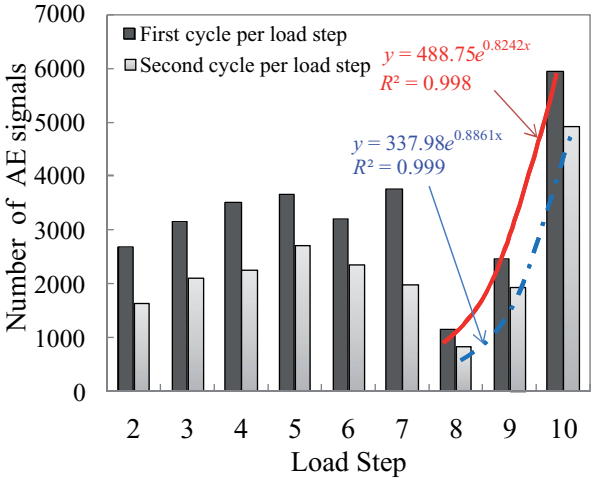

Figure 7. Variation of the number of AE signals during the test.
AE: acoustic emission.

is superimposed. In Figure 6, it can be observed that the amplitude of the AE signals is in general higher during the first cycle (Figure 6(a)) of each LS than during the second one (Figure 6(b)). This can be explained by noting that the second cycle has the same peak displacement as the first. Therefore, it is likely that during the first cycle of each LS, AE signals are generated mostly by the creation of new cracks, which usually generate AE signals of large amplitude. On the contrary, during the second cycle, AE activity is mostly generated by aggregates crushing and propagation of the preexisting cracks, which produce AE signals of smaller amplitude. The total number of AE signals also needs to be considered during the loading sequence. In particular, the total number of AE signals depends on whether the reload sequence is causing damage. If the reloading does not damage the structure, the number of new AE signals will be much smaller than the first cycle. If reloading damages the structure, the number of AE signals is higher.[30] Figure 7 shows the total number of AE signals recorded during the test. In particular, it can be observed that the total number of AE signals generated during the first cycle of each LS is larger than during the second one. This observation confirms that in each LS, the reloading does not damage the structure significantly but mostly cause reopening of cracks generated during the first cycle. Furthermore, an overall increase in the total number of AE signals recorded between the LS2 and the LS7 can be observed, which is likely to be related to the accumulation of damage during this stage. Interestingly, reduced AE activity was observed in the subsequent LS8 in which the onset of nonlinearity was observed. This can be explained by the fact that in this phase, AE signals were mostly generated by the propagation of macrocracks that usually generate few AE signals but of large amplitude. From this LS onward, the AE activity increased exponentially until the last LS when the wall lost significant strength.[19] The proximity of R^2 value to 1 verifies a relatively accurate correlation with number of AE signals and exponential functions superimposed on Figure 7 for both first and second cycles.

b-value results

To investigate the fracture process of the specimen during the test, a *b*-value analysis was carried out, as explained in section "Introduction to *b*-value analysis." Figure 8 shows the mean and standard deviation of *b*-values calculated during the loading process of each cycle. In particular, considering that each cycle consists of PLP and NLP (Figure 1), the *b*-value was calculated

Table 2. Average of *b*-values during the loading and unloading steps

Crack status	Loading			Unloading		
	PLP	NLP	Mean	PLP	NLP	Mean
Barely visible	1.31	1.16	1.23	1.63	1.52	1.55
Visible	1.13	1.13	1.13	1.25	0.96	1.09
Critical	1.10	0.84	0.96	1.06	0.70	0.87

PLP: positive load peak; NLP: negative load peak.

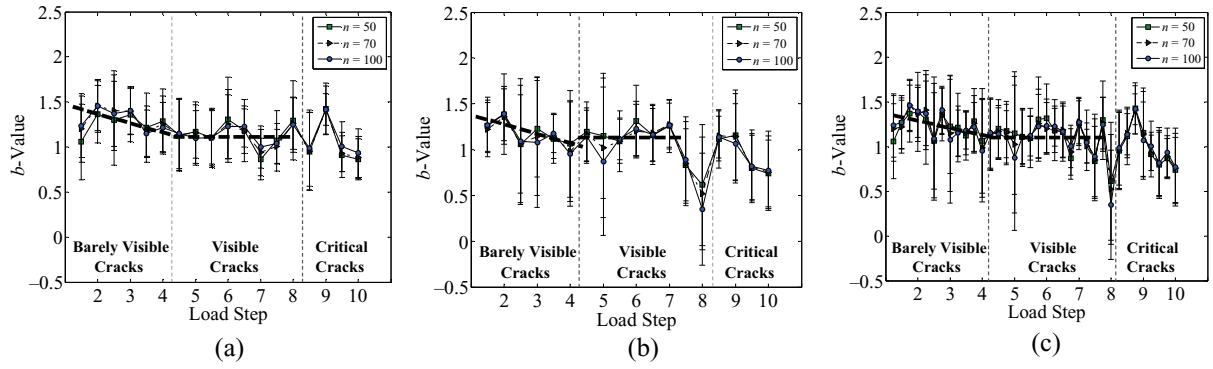

Figure 8. Variation of *b*-value and standard deviation during loadings by load step: (a) for PLPs, (b) for NLPs, and (c) for PLPs and NLPs consecutively.
PLP: positive load peak; NLP: negative load peak.

separately during these two phases as shown in Figure 8(a) and (b). For clarity, Figure 8(c) superposes these results. In Figure 8, an overall decreasing of *b*-values can be observed prior to LS5 followed by a relatively constant trend until LS7 with the minimum value obtained in the LS8-NLP. At this point, the applied load was approximately 81% of the peak capacity and the lateral stiffness had reduced to the 50% of the stiffness in LS2 (see Table 1). Interestingly, there was no evidence of critical damage from a normal visual inspection (see Figure 5). Figure 9 shows the mean and standard deviation of *b*-values calculated during the unloading process of each cycle. Also, in this case, the *b*-value was calculated separately during these two phases of PLP and NLP. A similar trend can be observed during the unloading phases of each cycle (Figure 9) but the slope of reduction in the initial unloading steps is larger and the minimum value occurred in LS9. Therefore, the *b*-value analysis reached its minimum value when the shear wall lost its ability to perform linearly as designed (see Figure 4(b)). Table 2 summarizes the results of the *b*-value analysis during the loading and unloading phases. In this article, it is defined as "barely visible cracks" a condition in which the maximum and modal (i.e. the most frequent) cracks widths are less than 0.3 and 0.2 mm, respectively; as "visible cracks" if they are less than 0.5 and 0.4 mm, respectively; and as "critical cracks" if they are larger than 1.5 and 0.4 mm, respectively. More details about cracks location, orientation, and width are available in Ref. 15.

It can be observed that the mean value, in the LSs in which the cracks were barely visible (i.e. LS1, LS2, LS3, LS4), is about 1.23 in the loading phases and 1.55 in the unloading ones. Considering that during the unloading phase, AE activity was mostly generated by the crushing of aggregates or concrete–rebar friction, whereas during the loading one, it was mostly dominated by cracks formation, this difference indicates that in the early stages of the load protocol, the amplitude of signals generated from cracks formation was higher than that of crushing of aggregates or concrete–rebar friction. However, there is no significant difference in the stage of visible cracks (i.e. 1.13 and 1.09). Finally, these values were smaller than 1 (i.e. 0.96 and 0.87) during the last LSs in which the specimen was visibly damaged (i.e. LS9, LS10). These results suggest that a threshold of $b = 1$ might be used to discriminate critical structural conditions; however, strong fluctuation on the *b*-value analysis (see Figures 8 and 9) might significantly increase the likelihood of false positives. A *b*-value–based outlier analysis is proposed in this article to reduce the number of false positive during a real-time monitoring of an RC shear wall.

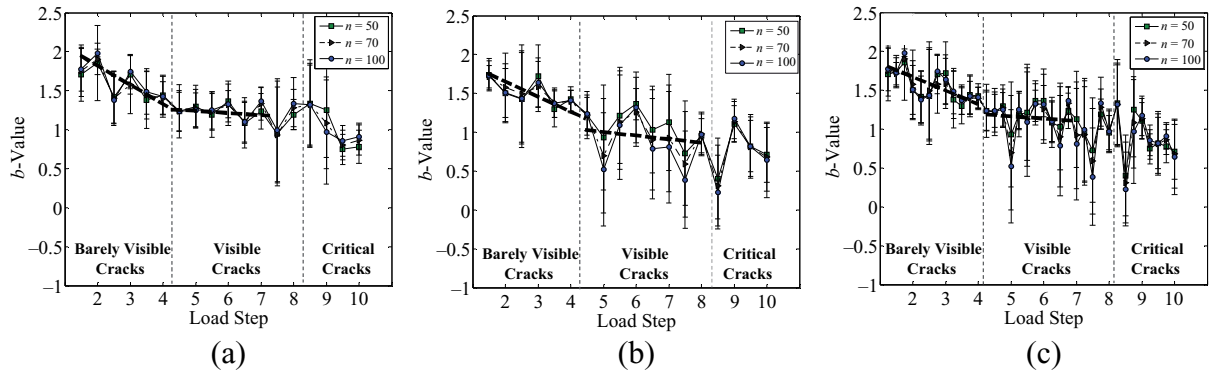

Figure 9. Variation of *b*-value and standard deviation during unloadings by load step: (a) for PLPs, (b) for NLPs, and (c) for PLPs and NLPs consecutively.
PLP: positive load peak; NLP: negative load peak.

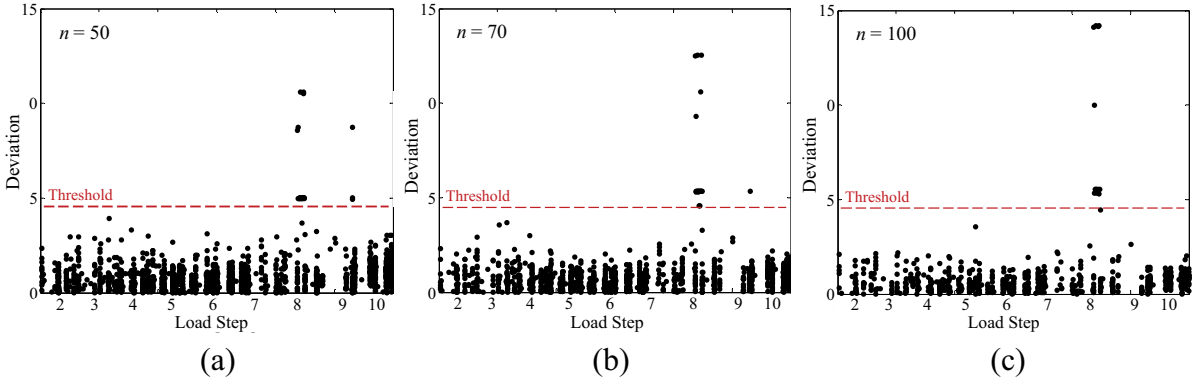

Figure 10. Outlier analysis results: (a) $n = 50$, (b) $n = 70$ and (c) $n = 100$.

Outlier analysis results

The results of the outlier analyses using the discordancy test based on deviation statistics defined in equation (3) are illustrated in Figure 10 for *b*-values calculated using groups of different sizes (i.e. $n = 50$, $n = 70$, and $n = 100$). The horizontal line is the value of a threshold representing the 99.9% confidence calculated by a Monte Carlo simulation. Definition of the threshold by the Monte Carlo method sometimes assumes that the baseline data are normally distributed. The Kolmogorov–Smirnov test[29] was computed to verify the Gaussian distribution of the baseline data. As can be observed the outlier analysis performed well in distinguishing *b*-values generated by critical conditions for the wall. In fact, the highest values of the discordance test were obtained at the point in which the shear wall lost its ability to perform linearly (i.e. LS8). In addition, the results were independent of the group size *n* used to calculate the *b*-value. In fact, in all three cases considered, the proposed algorithm was able to automatically classify as outliers the signals received in LS8. Therefore, the *b*-value–based outlier analysis was able to detect when the shear wall was not able to perform as designed and could provide a warning prior to complete failure of the structure.

Summary and conclusions

Postearthquake quick damage inspection of buildings is an essential step immediately after a major earthquake to guard against life loss in aftershocks. Visual inspection is the most common form of evaluation. However, there may be no outward signs that a structure has been significantly damaged after the main shock for which collapse might be imminent.[31–33] This work has proposed an SHM system capable of providing a rapid and automated damage assessment of an RC shear wall instrumented with an AE system prior to a significant event. The proposed system would be able to operate in a dual monitoring mode: (a) real-time continuous and (b) routine-based inspections. The system is based on a sparse array of AE sensors and a

statistical pattern recognition algorithm based on an outlier analysis to continuously monitor the structure under investigation. Experimental tests were carried out on a large-scale RC rectangular shear wall to validate the proposed SHM system. The specimen was subjected to multiple load cycles of increasing magnitude leading to complete wall failure. AE monitoring was performed in real-time using an array of eight piezoelectric sensors. The proposed system was successfully employed to monitor the fracture process as well as to identify the instant in which the specimen exhibited a nonlinear response. The system could provide an early warning of the structure failure and could inform decision makers of the need for repair to ensure safe and reliable structural performance. The following observation and conclusions were obtained:

- In general, the AE activity increased exponentially when the specimen was close to the failure;
- *b*-value analysis can be used to follow the fracture process in RC shear walls but it seems difficult to produce conclusive results;
- The overall trend of the *b*-value analysis is not affected by the group size used for the calculation although the value might be subjected to strong fluctuations due to normal operational condition (i.e. temperature and environmental noise);
- *b*-value-based outlier analysis can be a reliable way to automatically identify critical damage conditions and reduce the likelihood of false alarm.

Funding

This study was financially supported by US National Science Foundation (NSF) under Grant No. CMMI-0829978.

Acknowledgements

The experiments presented herein could not have been completed without contributions from the staff of the Structural Engineering and Earthquake Simulation Laboratory (SEESL) of the State University of New York at Buffalo. The financial support and work of the SEESL staff are gratefully acknowledged. The authors also acknowledge the advice and help provided by the technical staff at the NEES Equipment Site at the University at Buffalo.

References

1. Grosse CU and Ohtsu M. *Acoustic emission testing—basics for research-applications in civil engineering*. Berlin and Heidelberg: Springer-Verlag, 2008.
2. Rens KL, Wipf TJ and Klaiber FW. Review of nondestructive evaluation techniques of civil infrastructure. *J Perform Constr Fac* 1997; 11(4): 152–160.
3. Salamone S, Veletzos MJ, Lanza Di Scalea F, et al. Detection of initial yield and onset of failure in bonded posttensioned concrete beams. *J Bridge Eng* 2012; 17(6): 1–9 .
4. Salamone S, Bartoli I, Phillips R, et al. Health monitoring of prestressing tendons in posttensioned concrete bridges. *J Transport Res Board* 2011; 2220: 21–27.
5. Ohno K and Ohtsu M. Crack classification in concrete based on acoustic emission. *Construct Build Mater* 2010; 24(12): 2339–2346.
6. Ohtsu MY and Ono K. A generalized theory of acoustic emission and green's function in a half space. *J Acoust Emiss* 1984; 3(1): 27–40.
7. Gutenberg B and Richter CF. Seismicity of the earth and associated phenomena. In: *Frequency and energy of earthquakes*. Princeton, NJ: Princeton University Press, 1949, pp. 17–19.
8. Hardy HR Jr. Application of acoustic emission techniques to rock mechanics research. *Am Soc Test Mater* 1972; 505: 41–83.
9. Colombo IS, Main IG and Forde MC. Assessing damage of reinforced concrete beam using 'b-value' analysis of acoustic emission signals. *J Mater Civil Eng* 2003; 15: 280–286.
10. Kurz JH. stress drop and stress redistribution in concrete quantified over time by the b-value analysis. *Struct Health Monit* 2006; 5(1): 69–81.
11. Shiotani T, Yuyuma S, Li Z, et al. Application of AE improved b-value to quantitative evaluation of fracture process in concrete materials. *J Acoust Emiss* 2001; 19: 118–133.
12. Carpinteri A, Lacidogna G, Niccolini G, et al. Critical defect size distributions in concrete structures detected by the acoustic emission technique. *Meccanica* 2007; 43(3): 349–363.
13. Schumacher T, Higgins CC and Lovejoy SC. Estimating operating load conditions on reinforced concrete highway bridges with b-value analysis from acoustic emission monitoring. *Struct Health Monit* 2010; 10(1): 17–32.
14. ACI Committee 318. *Building code requirements for structural concrete and commentary (ACI 318-08)*. 2008. American Concrete Institute (ACI) located in Farmington Hills, MI, USA. ISBN: 9780870312649.
15. Rocks JF. *Large scale testing of low aspect ratio reinforced concrete walls*. MSc Thesis, Department of Civil, Structural and Environmental Engineering, University at Buffalo, Buffalo, NY, 2011.
16. Carter DC and Holford KM. Strategic consideration for the AE monitoring of bridges: a discussion and case study. *Insight* 1998; 40(2): 112–116.
17. Holford KM and Lark RJ. Acoustic emission testing of bridges. In: Gongkang F (ed.) *Inspection and monitoring techniques for bridges and structures*. Cambridge: Woodhead Publishing Ltd, 2005. 183–215.
18. Miller RK and Hill E. Acoustic emission testing. In: Moore PO (ed.) *Nondestructive testing handbook*. 3rd ed., vol. 6. Columbus, OH: ASNT, 2005, pp. 1–25.
19. Shiotani T. Parameter analysis. In: Grosse CU and Ohtsu M (eds) *Acoustic emission testing*. Berlin and Heidelberg: Springer-Verlag, 2008, pp. 41–51.
20. Kurz JH, Finck F, Grosse CU, et al. Stress drop and stress redistribution in concrete quantified over time by the b-value analysis. *Struct Health Monit* 2006; 5(1): 69–81.

21. Rizzo P, Cammarata M, Bartoli I, et al. Ultrasonic guided waves-based monitoring of rail head: laboratory and field tests (Article ID 291293). *Adv Civ Eng* 2010; 13 pp.
22. Rizzo P, Sorrivi E, Lanza Di Scalea F, et al. Wavelet-based outlier analysis for guided wave structural monitoring: application to multi-wire strands. *J Sound Vib* 2007; 307: 52–68.
23. Rizzo P, Cammarata M, Dutta D, et al. An unsupervised learning algorithm for fatigue crack detection in waveguides. *Smart Mater Struct* 2009; 18: 025016 (11 pp).
24. Salamone S, Lanza di Scalea F and Bartoli I. Damage detection in UAV wing skin-to-spar joints based on outlier analysis of guided wave energy. *J Intel Mater Syst Str* 2009; 20(9): 1079–1090.
25. Bartoli I, Salamone S, Phillips R, et al. Use of interwire ultrasonic leakage to quantify loss of prestress in multi-wire tendons. *J Eng Mech* 2011; 135(5): 324–334.
26. Barnett V and Lewis T. *Outliers in statistical data*. 3rd ed. Chichester, UK, John Wiley & Sons Ltd, 1994, pp. 52–171.
27. Worden K, Manson G and Fieller NRJ. Damage detection using outlier analysis. *J Sound Vib* 2000; 229(3): 647–667.
28. Luna BN. *Seismic response of low aspect ratio reinforced concrete walls for building and safety-related nuclear applications*. PhD Dissertation, Department of Civil, Structural and Environmental Engineering, University at Buffalo, NY, in preparation.
29. Massey FJ. The Kolmogorov-Smirnov test for goodness of fit. *J Am Stat Assoc* 1951; 46(253): 68–78.
30. Huston D. *Structural sensing, health monitoring, and performance evaluation*. Boca Raton, FL, USA, Taylor & Francis, 2011.
31. Holzer T. L., Barka A. A., Carver D., et al., USGS Circular 1193: implications for earthquake risk reduction in the United States from the Kocaeli, Turkey, earthquake of August 17, 1999, U.S. Geological Survey, Denver, CO, USA, 2000.
32. Comerio M, Elwood K, Berkowitz R et al., *The M 6.3 Christchurch, New Zealand, Earthquake of February 22, 2011*. EERI Special Earthquake Report. Earthquake Engineering Research Institute (EERI), Oakland, California, USA, May 2011. http://www.eeri.org/site/images/eeri_newsletter/2011_pdf/EERI_NewZealand_EQRpt_web.pdf
33. Kam WY, Akguzel U and Pampanin S. *4 weeks on: preliminary reconnaissance report from the Christchurch 22 Feb 2011 6.3MW earthquake*. Report from New Zealand Society for Earthquake Engineering Inc., 2011. 8 April 2011, New Zealand Society for Earthquake Engineering (NZSEE), Christchurch Earthquake Clearinghouse, New Zealand.